# SCN11A Gene Deletion Causes Sensorineural Hearing Loss by Impairing the Ribbon Synapses and Auditory Nerves

**Mian Zu**
Chinese PLA General Hospital
**Wei-wei Guo**
Chinese PLA General Hospital
**Tao Cong**
Chinese PLA General Hospital
**Fei Ji**
Chinese PLA General Hospital
**Shi-li Zhang**
Xuzhou Medical University
**Yue Zhang**
Chinese PLA General Hospital
**Xin Song**
Chinese PLA General Hospital
**Wei Sun**
University at Buffalo - The State University of New York
**David Z.Z. He**
Creighton University School of Medicine
**Wei-guo Shi**
Academy of Military Medical Sciences Institute of Pharmacology and Toxicology
**Shiming Yang** ( shm_yang@163.com )
Chinese PLA Medical School https://orcid.org/0000-0003-1860-8156

**Research article**

**Keywords:** TTX resistant sodium channels, expression, Nav1.9 knockout, ribbon synapse, SGN, progressive hearing loss, synaptopathy

**Posted Date:** September 22nd, 2020

**DOI:** https://doi.org/10.21203/rs.3.rs-46143/v1

**Version of Record:** A version of this preprint was published on March 22nd, 2021. See the published version at https://doi.org/10.1186/s12868-021-00613-8.

# Abstract

**Background:** The *SCN11A* gene, encoded Nav1.9 TTX resistant sodium channels, is a main effector in peripheral inflammation related pain in nociceptive neurons. The role of *SCN11A* gene in the auditory system has not been well characterized. We therefore examined the expression of *SCN11A* in the murine cochlea, the morphological and physiological features of Nav1.9 knockout (KO) ICR mice.

**Results:** Nav1.9 expression was found in the primary afferent endings beneath the inner hair cells (IHCs). The relative quantitative expression of Nav1.9 mRNA in modiolus of wild-type (WT) mice remains unchanged from P0 to P60. The number of presynaptic CtBP2 puncta in Nav1.9 KO mice was significantly lower than WT. In addition, the number of SGNs in Nav1.9 KO mice in the basal turn was also lower than WT, but not in the apical and middle turns. There was no lesion in the somas and stereocilia of hair cells in Nav1.9 KO mice. Nav1.9 KO mice showed higher and progressive ABR threshold at 16 kHz, a significant increase in CAP thresholds, while no changes in cochlear microphonics (CM).

**Conclusions:** These data suggest a role of Nav1.9 in regulating the function of ribbon synapses and the auditory nerves. The impairment induced by Nav1.9 gene deletion mimics the characters of cochlear synaptopathy.


# Highlights

Nav1.9 is expressed in SGN somata, nerve terminals, spiral and radial fibers in mouse cochlea.

*SCN11A* gene knockout causes gradually deteriorative hearing loss at 16 kHz.

*SCN11A* gene knockout causes reduced number of presynaptic CtBP2 puncta and SGN somata in the basal turn.

No significant hair cell loss occurred in *SCN11A* knockout mice.

# Background

The Nav1.9 sodium channel, encoded by *SCN11A* gene, was first identified in 1996 as an unusual voltage-gated sodium channel called SNS [1]. The Nav1.9 channel is well known for its presence in small-diameter nociceptive neurons dorsal root ganglion (DRG) [2, 3], trigeminal ganglia [4, 5] and myenteric intrinsic primary afferent neurons [6]. Recent studies found that Nav1.9 channel also expressed in photoreceptors and Muller glia in the visual system [7]. Nav1.9 shares only 50% identity with the other voltage-gated $Na^+$ channel isoforms, but it doesn't belong to a new Nav subfamily according to phylogeny [8]. Nav1.9 carries a serine (S) residue in the DI-SS2 pore region, rather than a tyrosine (Y) or a phenylalanine (F), which markedly reduces the affinity of the TTX-channel interaction by more than 200-fold [9].

Nav1.9 typically exhibits ultra-slow kinetics with an activation at around − 65 mV, lower than Nav1.1, a TTX sensitive sodium channel [10], the consolidation of which is important for the maturation of afferent fiber in the weeks after hearing onset. Unlike Nav1.1, Nav1.9 does not contribute so much to the amplitude of action potential, but facilitate excitation of small depolarization by amplifying receptor potentials. The 'ultra-slow' inactivation of Nav1.9 renders the persistence of the sodium current after activation, corresponding to a wide range of voltage to keep a persistently open channel close to the resting membrane potential [11]. The biophysical properties of Nav1.9 channels suggest their probable contribution to prolonging the response to a subthreshold stimulus and supporting repetitive firing [12].

Nav1.9 mediates tissue-damage in DRG with unmyelinated C fibers by transforming receptor potentials into action potentials. Nav1.9 KO mice shows less stimulation-induced calcitonin gene-related peptide (CGRP) release form skin, which implys that Nav1.9 has a role in modulating neurotransmitter release from afferent nerve endings [13]. Cochlea includes two types of auditory nerves. Type I afferents are myelinated innervating to IHCs, while Type II afferents are unmyelinated innervating outer hair cells (OHCs). Type II afferents may be the cochlea's nociceptors, as highly enriched gene ontology (GO) terms in type II neurons (*Prph+, Th+*), were associated with "response to stress" and "pain" by single cell RNA-seq sequencing [14].

Multiple TTX-sensitive $Na^+$ currents, including a subthreshold persistent $Na^+$ current ($I_{NaP}$), a resurgent $Na^+$ current ($I_{NaR}$) and fast inward sodium currents, could be recorded in cultured SGNs after the onset of hearing, while the function of Nav1.9 in auditory sensory system remains enigmatic. [15, 16]. The gene expression microarray shows that, *SCN11a* shares a similar pattern with atonal homolog 1a (*Atoh1*) during hair cell differentiation, which is a well-known factor during inner ear development [17]. The relative expression level of *SCN11a* in cochlea is 1.7 compared with that of Atoh1 as 5.2 [18]. Moreover, Nav1.9 protein is expressed in cartwheel cells (CWCs) in the dorsal cochlear nucleus (DCN). And Nav1.9 is proved to contribute to respond with compound action potential (CAP) containing single action potentials (SAPs) superimposed on a slow depolarization[19].

In this paper we studied the expression and function Nav1.9 in the cochlea of mice. We found abnormal ABRs and CAPs, as well as decreased presynaptic CtBP2 puncta and SGN in Nav1.9 KO mice, suggesting impairment of the auditory signal transmission. Nav1.9 may contribute to auditory neurotransmission, sharing a similar protein expression pattern in nociceptive neurons of DRG as an effector of peripheral pain hypersensitivity.

# Methods

All animal procedures were carried out in accordance with the Policy on Human Care and Use of Laboratory Animals at PLA General Hospital and approved by the Institutional Animal Care and Use Committee (process no. 2018-X14-84).

# Construction of Nav1.9$^{-/-}$ mice using CRISPR/Cas9

Nav1.9$^{-/-}$ ICR mice were obtained from CasGene Biotech.Co., Ltd. The specific single-guide RNAs (gRNAs) were designed and synthesized (gRNA1: ccctgtagtcgtttgaaggttag; gRNA2: cccattccgcgaccagctgtggc). To generate Nav1.9 knockout mice, gRNAs targeting a section of the *SCN11A* gene encoding sequence beside the PAM sequence, and Cas9 nucleases could introduce a double-strand break (DSB) (**Fig. 1**). The all-in-one plasmid expressing Cas9 and gRNA was microinjected into fertilized eggs under micromanipulation. About 3 weeks after the injection of eggs to a pseudopregnant female, the founder mice were obtained. The homologous genetic deletion was identified by PCR amplification (forward primer: 5'-GACACTCTGGCGGT GCCTTCC-3'; KO specific reverse primer: 5'-TTGCTCCCACCTTACCAATACAGACTC-3'; WT specific reverse primer: 5'-CGACATTCCTCCGAGACCTGTTAGA-3') and DNA sequencing analysis. The off-target effect and germline transmission to the offspring were then determined. Heterozygous males and females were mated to produce wildtype, heterozygous and homozygous offspring. Mice were maintained in a humidity and temperature-controlled IVC animal experiment system with 12 h light/dark cycle.

# Real-time quantitative PCR

Real-time quantitative PCR (qPCR) was used to identify mRNA expression of Nav1.9 in cochlea of mice at different time points after birth (P0, P7, P14, P21, P28 and P60), with five mice in each group. Total RNA from modiolus was prepared by RNeasy Mini Kit (cat. 74104, QIAGEN) followed by purity determination and quantitation. cDNA was synthesized by random primer using the TransScript first-strand synthesis supermix for RT-PCR (TransGen Biotech). qPCR with reaction volume of 20 μL containing primers (200 nM) and 1 μL cDNA, was performed on CFX96$^{TM}$ Real-Time PCR Detection Systems (Bio-Rad Life Science). Specific primers for Nav1.9, Nav1.1 and GAPDH (housekeeping gene) were designed and synthesized (**Tab. 1**). The following run protocol for amplification was used: denaturation (94℃ for 30s), amplification and quantification by 45 cycles (94℃ for 5s, 56.8℃ for 15s, 72℃ for 10s), melting curve (65-95℃ with a heating rate of 0.1℃/s). Negative controls with Ct values more than 38 or no visible amplification curve were tested in each run. The relative expression level was calculated by the $2^{-\Delta\Delta Ct}$ method as previously described [20, 21].

Table 1

Primers for real-time RT-PCR analysis

| Target | Sequence (5’ to 3’) | |
|---|---|---|
| | Forward primer | Reverse primer |
| Nav1.1 | TTCAGGGGCTATCGAGGC | TGCTGAATAATGAGTGTACCAAAAT |
| Nav1.9 | GAAAAAGTTAGGTGGCCAAGACAT | GTTGGGCTGGCCTTCAGATT |
| GAPDH | GGAATGCCTACCTTGCCCTG | ATGTCTTGGCCACCTAACTTTT |

# Cochlea sectioning and scanning electron microscopy (SEM)

After the anesthesia by an intraperitoneal injection of pentobarbital sodium (50 mg/Kg), the P60-adult mice were sacrificed by decapitation. The cochleas were isolated and fixed in 4% paraformaldehyde overnight, followed by decalcification in 10% EDTA at room temperature for 24h. For cochlea immunostaining, the tissues were cryoprotected successively in 20% and 30% sucrose in PBS for 2h and in Tissue Freezing Medium (OCT) at 4℃ until they sank. The cryoprotected tissues were sectioned at 10 μm for immunostaining, while sections at 2 μm were prepared for hematoxylin and eosin staining,.

For the SEM, the cochlea was perfused and fixed with 2.5% glutaraldehyde. After decalcified in 10% EDTA, cochleas were post-fixed with 1% osmium tetroxide, dehydrated and embedded on aluminum stubs, coated with gold particles.

# Immunohistochemistry and synaptic counts

After washes with 0.1% Triton X-100 in PBS, sections on adhesive-precoated glass slides were blocked with 10% normal goat serum (ZLI-9021, ZSGB-BIO) and incubated with rabbit anti-*SCN11A* polyclonal antibody (AT322395, 1:200, OriGene, Rockville, MD), guinea pig anti-Nav1.9 polyclonal antibody (AGP-030, 1:200, alomone labs, Israel), mouse anti-CtBP2 (612044, 1:100, BD Biosciences), anti-hypophosphorylated neurofilament H antibody (ab82259, 1:100, abcam) in 10% goat serum diluted in 0.1 M PBS at 4℃ overnight and then incubated with secondary antibodies containing anti-mouse Alexa Fluor™ 488 (lot 1810918 ,1:400, goat, Thermo Fisher), anti-rabbit Alexa Fluor™ 568 (lot 1494753 ,1:400, goat, Thermo Fisher), or anti- guinea pig Alexa Fluro™647 (A-21450 ,1:400, goat, Thermo Fisher). Cell nuclei were labeled by DAPI.

For pre-synaptic ribbons counts, all pieces of each basilar membrane for each mouse were imaged with converted locations into frequency by ImageJ Plugin according to Cochlear Frequency Mapping in Whole Mounts (MASSACHUSETTS EYE AND EAR). Confocal z stacks from 4.0 to 64.0 kHz regions form each cochlea were taken using a LEICA DMi8 microscope equipped with 63×oil immersion lens. Five random fields at the region of 20-50% (mouse standardized cochleogram according to Müller (2004)) from the

apex were chosen for pre-synaptic ribbons counting, corresponding to the frequency around 8-16 kHz. The z stacks with 10 μm (0.75 μm step size) were set to ensure all the synaptic specializations were imaged. CtBP2 puncta in superimposed confocal z stacks was visualized and counted as presynaptic counts for each IHC. Each image usually contained 17-25 IHCs[22].

# Haematoxylin Eosin (H&E) staining and SGN counting

The sections were deparaffinized with xylene twice (10 min each), followed by re-hydration in 2 changes of absolute alcohol (5 min each), 95% alcohol, 85% alcohol, 75% alcohol (2 min each) and washed in distilled water briefly. Then the sections were stained in Harris hematoxylin solution and counterstained in eosin-phloxine solution. The sections were dehydrated through 95% alcohol and absolute alcohol and cleared in xylene twice, 5 min for each time. Finally, the mounted sections were observed under a light microscope[23].

The established method of paraffin slide was used for auditory neuron count[24]. In 5 mid-modiolar slices per cochlea from paraffin-embedding tissue, with 2 μm each on every 5th section, the perimeters of Rosenthal's Canal were surveyed and the mean cell number of 5 slices was regarded as neuron count for one mouse. The number of SGNs with soma diameter equal or greater than 13 μm within the apex, middle and basal modiolus were chosen and counted manually with the assistant of Image J, respectively[25].

# Western blot analysis

Protein lysate from bilateral cochlea samples for each mouse was prepared in RIPA lysis buffer with the adding of complete protease inhibitor by Tissue Grinding Pestles, followed by keeping in an ice bath for 10 min. After centrifugation at 12,000 rpm for 10 min at 4℃, the supernatant mixed with loading buffer was denatured and loaded on a SDS-PAGE (12%) gel. Proteins were transferred to PVDF membrane for 90 min in an ice bath. After blocking, the membrane was incubated in primary antibodies of anti-Nav1.9 and anti-β actin with gentle agitation at 4℃ overnight, followed by HRP-conjugated secondary antibody incubation. Finally, the signal of HRP was detected using GE Healthcare's ECL detection reagent. Antibodies in this study were as follows: polyclonal rabbit anti-SCN11A polyclonal antibody (AT322395, 1:1000, OriGene), beta Actin mouse monoclonal antibody (TA811000, 1:1000, OriGene), anti-rabbit HRP-linked IgG (7074, 1:4000, Cell Signaling Technology), goat anti-mouse HRP-linked IgG (H+L) (LK2003, 1:4000, sungene biotech).

# Auditory brainstem response (ABR) and ECochG recording

Mice were anesthetized using an intraperitoneal injection of pentobarbital sodium (50 mg/Kg) and kept on a thermal insulation blanket. Click stimuli or pure tone stimuli from 2 to 16 kHz were generated by

Tucker Davis Technologies System (TDT) and delivered by a MF1 speaker (TDT)[26]. The intensity of the tone stimuli was calibrated using a sound level meter with 1/4-inch pressure-field microphone (B&K). Response signals were recorded with needle electrodes subcutaneously inserted at the scalp vertex, the postauricular region of the ipsilateral ear as reference, and the contralateral ear as ground. Auditory thresholds were determined as the lowest sound intensity with reproducible and recognizable waves by decreasing the sound intensity from 100 to 10 dB SPL in 5 dB steps. Mean±SD was plotted as a function of stimulating sound frequencies, or a function of months after birth at one frequency for each genotype[27].

For ECochG recordings, left cochlea was exposed through a dorsolateral posterior-auricular surgical approach. Once the bulla had been opened by a cutting burr, the recording electrode was placed on the round window membrane with the aid of a micromanipulator. The reference and ground electrodes were placed in the muscle near the cochlea. When the CAP of the auditory nerve was probed, the acoustical stimuli were generated by TDT system and delivery to a MF1 speaker. A sine-wave generator was adjusted to phase-locked for CM stimulus. Stimuli were shaped and timed as follow: 400 us rise and decay time, 4 ms duration. The responses of 2 month-old of WT or Nav1.9$^{-/-}$ mice, evoked by phase-locked 100 to 10 dB, 4 kHz tone bursts in the CM mode (bioelectrical signal bandpassed from 3 to 5 kHz), were recorded. Cochlear amplification was achieved through an amplifier, averaged 1024 times. The CAPs were evoked at 16 kHz tone burst and threshold was obtained. The amplitude and latency of the first positive peak (P1) amplitude were measured. All experiments were carried out in a double-walled sound-attenuating room.

# Statistical analysis

Data was analyzed by SPSS version 17.0 software (SPSS Inc., Chicago, IL, USA) and plotted using GraphPad prism 7 (Graphpad, USA), and expressed as mean±SD. Quantitative data statistical analysis was performed by one-way ANOVA followed by post-hoc tests (as appropriate) for multiple group comparisons, independent samples *t* test and nonparametric test (Mann-Whitney U test) for two-group data. $^{*}p<0.05$, $^{**}p<0.01$ and $^{***}p<0.001$ were considered to indicate a statistically significance.

# Results

# Disruption of *SCN11A*

Nav1.9 KO mice were genotyped by PCR using genomic DNA from ear marginal tissue. Primer pair 1 and primer pair 2 was used to specifically distinguish WT and Nav1.9$^{-/-}$ genotypes. The resulting products of WT, Nav1.9$^{+/-}$ and Nav1.9$^{-/-}$ were analyzed by agarose gel electrophoresis (**Fig. 2A**). The deletion of 347 bp, starting in exon 3 and ending in exon 5 of the coding sequence of *SCN11A* mRNA, induced a truncated form of Nav1.9 with 96 amino acid residues, and led to the reading frame shift mutation followed by a premature translational-termination codon (**Fig. 2B**). The mutation resulted in dysfunction

of the protein with no membrane-spanning domain. No significant phenotypic difference was found in Nav1.9$^{-/-}$ mice from WT littermates in their size, weight, coat color, locomotor activity, eating or drinking behavior, fertility and life span. Besides, necropsy and histology between Nav1.9$^{-/-}$ and WT mice were considered indistinguishable, apart from a poor protein expression of Nav1.9 in the cochlea of Nav1.9$^{-/-}$ mice (**Fig. 2C**).

# Nav1.9 is expressed in the inner ear and auditory pathway of wild-type mice

The expression of Nav1.1 and Nav1.9 mRNA from modiolus was examined using qPCR in WT mice from P0-P60 (5 mice in each time point). During cochlea development, the expression of Nav1.9 showed no significant difference at P7, P14, P28 and P60 (**Fig. 3A**, one-way ANOVA, $F$=1.673, $p$=0.18). However, the relative expression levels of Nav1.1 mRNA at P14 and P60 were significantly higher than that at P0 (**Fig. 3A**, one-way ANOVA with Tamhane's post-hoc test, $^{*}p$=0.028, $^{**}p$=0.004).

The localization of Nav1.9 in the cochlea was primary afferent and efferent endings in the organ of Corti, SGN somata and cochlear nucleus (**Fig. 3B**). It was found that, in mouse cochlea, Nav1.9 immunoreactivity was located in inner spiral fibers beneath the inner hair cells (IHCs), radial fibers innervating IHCs, tunnel crossing fibers and outer radial fibers (**Fig. 3C c1 c3 and c4**), according to the diagram of the cochlea's afferent innervations pattern from Ballenger'S OTORHINOLARYNGOLOGY 18 (**Fig. 3C c2**). Nav1.9 immunoreactivity was present in a small number of neurons, which couldn't be stained by anti-MBP antibody, a marker labeling myelin sheath (**Fig. 3D and Fig. S3**). Some neurons within the cochlear nucleus exhibited expression of Nav1.9 on cell membranes at a relatively low density (**Fig. 3E**), which was consistent with data from previous studies [19].

# Nav1.9$^{-/-}$ mice are deaf progressively at 16 kHz

ABR was used to assess hearing thresholds in 2-month-old mice. The averaged ABR thresholds of Nav1.9$^{+/+}$ mice Nav1.9$^{+/-}$ mice and Nav1.9$^{-/-}$ mice showed no significant difference with each other at 2 kHz (**Fig. 4A,** one-way ANOVA, $F$=2.954, $p$=0.085) and 8 kHz (**Fig. 4A,** one-way ANOVA, $F$=0.576, $p$=0.571), respectively (**Tab. 2**). In addition, Nav1.9$^{-/-}$ mice (n=7) showed a remarkably higher average ABR threshold than Nav1.9$^{+/-}$ (n=4) and WT mice (n=6) by 36.8 dB SPL ($^{**}p$=0.002) and 38.3 dB SPL ($^{**}p$=0.001) at 12 kHz (**Fig. 4A,** one-way ANOVA with Bonferroni's post-hoc test), respectively. The average ABR threshold of Nav1.9$^{-/-}$ mice was up to 78.9 ± 10.5 dB SPL, which is significantly higher than Nav1.9$^{+/-}$ (58.8±14.9 dB SPL) ($^{*}p$ = 0.01) and WT mice (41.7 ±6.6 dB SPL) ($^{***}p$=0.000) at 16 kHz, while the average ABR threshold of Nav1.9$^{+/-}$ was higher than WT mice ($^{*}p$=0.032) (**Fig. 4A,** one-way ANOVA with Bonferroni's post-hoc test) as well. In all mice tested, threshold elevation correlated with reduced amplitudes of all ABR waves at 16 kHz were found in Nav1.9$^{-/-}$ mice (**Fig. 4B**).

Table 2

ABR thresholds in Nav1.9$^{+/+, +/-, -/-}$ mice at 2 months of age

| Group | Frequency (kHz) | | | |
|---|---|---|---|---|
| | 2 | 8 | 12 | 16 |
| Nav1.9+/+ | 57.5 ± 9.9 | 39.0 ± 8.1 | 41.0 ± 11.4** | 41.7 ± 6.6*** |
| Nav1.9+/- | 70.0 ± 7.1 | 42.5 ± 15.5 | 42.5 ± 15.0** | 58.8 ± 14.9* |
| Nav1.9-/- | 70.0 ± 11.5 | 36.7 ± 6.6 | 79.3 ± 13.7 | 78.9 ± 10.5 |

To examine the onset time of hearing loss, ABR thresholds at the P21, P30, and P60 were measured at 8 and 16 kHz, respectively. At 8 kHz, the average ABR thresholds of WT mice was 38.7 ± 5.5 (n =15) at P21 and 39.0 ± 8.1 dB SPL (n = 10) at P60. The ABR thresholds of Nav1.9$^{-/-}$ mice was 39.3 ± 5.3 dB SPL (n=7) at P21 and 36.7 ± 6.6 dB SPL (n=9) at P60. There was no significant difference between the WT and KO mice (**Fig. 4C,** $t$=-0.248, $p$=0.807 at P21; $t$=0.087, $p$=0.932 at P30; $t$=0.683, $p$=0.504 at P60 with independent samples $t$ test); At 16 kHz, the ABR threshold of WT mice was 30.0 ± 8.5 dB SPL (n=15) at P21, which was significantly lower than their Nav1.9$^{-/-}$ littermates of 44.3 ± 8.9 dB SPL (n=7) ($U$=14.5, $Z$=-2.751, **$p$=0.006 with Mann-Whitney U test). Besides, the Nav1.9$^{-/-}$ mice showed a significant ABR threshold elevation compared with their WT littermates at P30 (72.9 ± 17.5 dB SPL (n=12) vs 40.0 ± 9.1 dB SPL (n=4), $U$=4.5, $Z$=-2.406, *$p$=0.016 with Mann-Whitney U test **Fig. 4D**), and at P60 (78.9 ± 10.5 dB SPL (n=9) vs 41.7 ± 6.6 dB SPL (n=9), $U$=0.000, $Z$=-3.608, ***$p$=0.000 with Mann-Whitney U test **Fig. 4D**). The ABR threshold shifts of Nav1.9$^{-/-}$ mice in comparison with WT littermates, were 14.3 dB SPL at P21, 32.9 dB SPL at P30, and 37.2 dB SPL at P60, respectively, exhibiting progressive hearing loss (**Tab. 3**).

Table 3

ABR thresholds in Nac1.9$^{+/+, -/-}$ mice at different age

| Age (Day) | 8K | | 16K | |
|---|---|---|---|---|
| | WT | Nav1.9$^{-/-}$ | WT | Nav1.9$^{-/-}$ |
| P21 | 38.7 ± 5.5 | 39.3 ± 5.3 | 30.0 ± 8.5 | 44.3 ± 8.9** |
| P30 | 37.5 ± 6.5 | 36.9 ± 13.3 | 40.0 ± 9.1 | 72.9 ± 17.5* |
| P60 | 39.0 ± 8.1 | 36.7 ± 6.6 | 41.7 ± 6.6 | 78.9 ± 10.5*** |

# CAP and CM recordings

In order to identify the lesion region of hearing loss affected by Nav1.9, the CAP was recorded from the round window of cochlea. The average threshold of CAP of Nav1.9$^{-/-}$ mice was 80.0±10.0 dB (n = 5) which was significantly higher than the WT mice (45.0±11.5 dB SPL, n=4) ($U$=0.000, $Z$=-2.491, $^{*}p$=0.013 with Mann-Whitney U test, **Fig. 5A**). The average amplitude in P1 wave of Nav1.9$^{-/-}$ mice at 80 dB SPL was 4.6±3.9 μV (n=5) which was significantly lower than that form the WT mice (22.1±15.6 μV, n=5), ($t$=2.434, $^{*}p$=0.041, independent samples $t$ test, **Fig. 5B**). In addition, the average latencies of P1 waves from WT and Nav1.9$^{-/-}$ mice were 2.1±0.4 ms (n=7) and 2.4±0.4 ms (n=5), respectively, with no statistical difference ($t$=-1.244, $p$=0.242 with independent samples $t$ test) (**Fig. 5C**). The representative CAP waveforms of WT and Nav1.9$^{-/-}$ were shown in **Fig. 5D** and **Fig. 5E**.

The CM responses at 4 kHz were recorded in the WT and KO mice followed the frequency and waveform of the sound stimuli. We recorded normal CMs from Nav1.9$^{-/-}$ mice (**Fig. 6A, 6B, 6C**). Difference in the CMs growth functions between WT and Nav1.9$^{-/-}$ mice was not significant. In all, these results led us to conclude that the hearing impairment observed in Nav1.9$^{-/-}$ mice qualifies as auditory neuropathy.

# Ribbon synapse counting

The quantitative changes in ribbon presynaptic RIBEYE were stained using antibodies against CtBP2. The average number of CtBP2 puncta in WT mice (n=7) was 7.3 ± 2.4 per IHC, which was statistically higher than that in Nav1.9$^{-/-}$ mice with 4.2 ± 1.6 per IHC (n=5) ($U$=4.5, $Z$=-2.122, $^{*}p$=0.034, Mann-Whitney U test, **Fig. 7A, 7B, 7C**). This data indicates that Nav1.9 KO induced auditory deficits by a mechanism including cochlear synaptopathy.

# SGN counting

The number of spiral ganglion neurons (SGNs) was counted. The average number of the SGNs in the basal turn of cochlea of Nav1.9$^{-/-}$ mice (n=4) was 37.0±3.1, which is significantly lower than that of WT

mice (n=5) with 51.0±5.8 ($U$=0.000, $Z$=-2.46, $^{*}p$=0.014, Mann-Whitney U test, **Fig. 7D, 7E, 7F**). However, the number of SGNs in both apical ($t$=0.518, $p$=0.622 with independent samples $t$ test) and middle turn ($t$=0.703, $p$=0.823 with independent samples $t$ test) showed no statistical difference between the two groups. The average numbers of SGN were 45.8 ± 4.7 in apex and 53.8±8.2 in middle for Nav1.9$^{-/-}$ mice; 48.3 ± 9.3 in apex and 54.6 ± 11.2 in middle for WT mice, which was in accordance with impaired temporal neural code at high frequency, such as 16 kHz.

# Nav1.9 knockout with intact OHCs

Nav1.9$^{-/-}$ mice had spared outer hair cells (OHCs) function of mechanoelectrical transduction and cochlear amplification, as evidenced by preserved cochlear microphonic potentials (CM). To explore the hair cell morphology in the region of ABR threshold shift, a standard cochleogram of a 4 months old Nav1.9$^{-/-}$ mouse was provided (**Fig. 8A)**, containing scales of frequency, percent distance from the apex according to Müller (2004) (**Fig. 8B)**. No significant hair cell missing from base to apex was found in cochleograms from DAPI stainging, especiall in the middle turn (30-55% distance from the apex) (**Fig. 8C)**. Subsequently, we investigated the morphology of inner and outer hair cell stereocilia by scanning electron microscopy. Adult Nav1.9$^{-/-}$ mice at 2 months had well-formed stereociliary bundles, with evenly spaced stereocilia within each bundle and an equal height within each row for the apical (**Fig. 8D**, **b1-b3**) and middle turn (**Fig. 8D**, **b4-b6**), the basal turn as well (**Fig. 8D**, **b7-b9**).

## Discussion

This paper we have three novel findings on the expression and function of Nav1.9 in auditory system. 1. Nav1.9 was detected in the cytomembrane of SGNs which can also be stained by peripherin; 2. Nav1.9 KO mice showed a high frequency hearing loss at 2 months age. 3. Morphology experiments demonstrated reduced synapses and number of auditory nerves in the basal turn of the cochlea in Nav1.9 KO mice.

# Nav1.9 is predominantly present in peripheral auditory nerve

We found that Nav1.9 was located in nerve terminals in a plane beneath the IHCs. Also stained are the afferent radial fibers leading through the foramina nervosa (FN) (Fig. S1), and a small part of SGNs somata, their peripheral and central initial segments. The distribution of Nav1.9 detected in the dorsal cochlear nucleus was consistent with a previous study [19]. In addition, Nav1.9 labeled fibers run longitudinally beneath the IHCs among scattered CtBP2 in the presynaptic membrane (Fig. S2), suggesting that this sodium channel may play a role in modulating neurotransmitter such as glutamic acid in presynaptic membrane. This hypothesis was consistent with less heat-induced calcitonin gene-related peptide release form the skin in Nav1.9 KO mice. Alternatively, Nav1.9 may affect the ribbon synapse plasticity as well.

The distribution of Nav1.9 in auditory afferent nerve is similar to that in functionally identified nociceptors [28]. The localization of Nav1.9 channels at primary afferent peripheral nerve endings in the skin, is in analogy to that in afferent nerve ending beneath the IHCs; Nav1.9 in DRG somata is in analogy to that in SGN somata; Nav1.9 is expressed in central nerve endings in the dorsal horn of the spinal cord, in analogy to that in dorsal cochlear nucleus. However, more evidences that Nav1.9 distributes in auditory primary afferent are still needed.

Furthermore, as one of Nav channels specifically expressed in the peripheral nervous system, Nav1.9 may be expressed with unique patterns. Unlike Nav1.6 which is localized in the outer spiral fibers and their sensory endings beneath the OHCs, and Nav1.2 which is localized to the unmyelinated efferent axons and their endings on the IHCs and OHCs, Nav1.9 is predominantly present in the inner spiral fibers beneath the IHCs, which consist of distinctive neuronal plexus (glutamic acid decarboxylase (GAD)-positive fibers and gamma-aminobutyric (GABA)-positive fibers) intimately associated with IHCs [29]. Compared with mRNA expression of Nav1.1, which is a main contributor to auditory nerve spike generation [30], the expression of Nav1.9 mRNA was much lower at P7 at the onset of hearing. The different expression profile of Nav1.9 with Nav1.1, suggests that this channel may contribute less to the action potentials generation. Third, Nav1.9 KO mice showed elevated CAP thresholds compared to the WT mice. Moreover, the decreased amplitudes of CAP may result from loss of neural activity, as a result of a decrease in SGN count in Nav1.9 KO mice. Therefore Nav1.9 channels may serve as an amplifier of receptor potentials, facilitating neuronal excitation, rather than contributing to action potential generation.

# Nav1.9 knockout mice show reduced ribbon synapses.

The average number of ribbon synapse in adult Nav1.9 KO mice was lower than their WT littermates. All synaptic ribbons contain a unique ribbon-specific scaffolding protein called RIBEYE, which contains a C-terminal B-domain that is identical with the transcription factor CtBP2 [31]. The reduced CtBP2 intensity in Nav1.9 KO mice suggests that Nav1.9 is essential for integrity of presynaptic nano-domains that position release-ready synaptic vesicles. An analogy to this hypothesis is the possible role of Nav1.9 in modulating neurotransmitter release in the dorsal horn of the spinal cord at the first synapse mediating pain signaling [28]. The mechanism of Nav1.9 in modulating morphology and function of ribbon synapse is still ambiguous. One candidate factor neurotrophin-3 (Ntf3) has been reported to regulate ribbon synapse density in the cochlea. Supporting cell-derived Ntf3 promotes ribbon synapse regeneration after acoustic trauma [32]. In the CCI model of neuropathic pain, Ntf3 is capable of attenuating expression of Nav1.9 mRNA and protein [33], indicating a possible ability of Ntf3 modulating the plasticity of ribbon synapse via Nav1.9 in cochlea.

Knockout of Nav1.9 induces postsynaptic degradation including loss of both ribbon synapse and SGNs, which may not affect the activity of OHCs. Although Nav1.9 distributes tunnel fibers to OHCs, knockout alleles doesn’t cause significant OHCs loss or dysfunction, due to the possible compensation of other sodium channels such as Nav1.2 or Nav1.6 tracking afferent innervation of OHCs [34].

# Nav1.9 knockout mice have progressive hearing loss in high frequency.

This study showed Nav1.9 knockout mice with profound hearing loss at 16 kHz as early as 1 month after birth, while at 8 kHz no significant acoustic trauma was found from 21 days to 2 months after birth. Redox imbalance induced progressive haring loss was explored in a *Dusp1* deficient mouse model, which progressively trigger inflammation and apoptotic cell death [35]. It is implied that Nav1.9 knockout may trigger a stress imbalance. In support of this hypothesis, the current density of Nav1.9 was increased by inflammatory mediators, such as interleukin-1β[36], thus rendering DRG neurons hyperexcitable and leading to pain in inflammatory disorders.

Hearing loss in high frequency may result from reduced SGNs in the basal turn by affecting the cellular survival or development in Nav1.9 knockout mice. One explanation may be that the neurotrophins neurotrohin-3 (NT-3) and brain-derived neurotrophic factor (BDNF) could regulate the gradient expression of Nav1.9 in the organ of Corti. Both BDNF and NT-3 expressed in the cochlea support SGN survival during development. As NT-3 expression is highest in the cochlear apex and lowest in the base, and high expression on the modiolar side, the negative regulation might contribute to the higher expression level of Nav1.9 in the base. BDNF, the receptor tyrosine kinase (TrkB) and Nav1.9 has been reported as a gating mechanism in both hippocampal neurons in CNS and SH-SY5Y line [9]. Nav1.9 knockout may have significant effect on the survival of SGN in the base, through reduction of BDNF-TrkB-Nav1.9 pathway. The exact mechanism why Nav1.9 knockout affected SGN survival in the basal turn, rather than the middle and apex, is still unclear.

## Conclusions

Our data provide the first evidence for the scientific hypothesis that Nav1.9 as a main contributor to human pain disorders in former study, is expressed in SGN neuronal somata, nerve terminals, spiral and radicl fibers in mouse cochlea. Moreover, our data show that deletion of *SCN11A* gene causes the emergence of the mutator phenotype of sensorineural hearing loss at frequency of 12 kHz to 16 kHz, aggravating gradually especially at 16 kHz. Finally, reduced number of presynaptic CtBP2 and SGN somata in the basal turn are found in Nav1.9 KO mice, suggesting that the channel could modulate neurotransmitter release from presynaptic membrane, as well as affect the cell survival of SGN. The precise mechanism of Nav1.9 in modulating auditory neural function is still the key challenge for the further study.

## Abbreviations

knockout: KO; spiral ganglion neurons: SGNs; auditory brainstem response: ABR; electrocochleogram recordings: ECochGs; inner hair cells: IHCs; outer hair cells: OHCs; wild-type: WT; cochlear microphonics: CM; compound action potential: CAP; single action potentials: SAPs; dorsal root ganglion: DRG; brain-derived neurotrophic factor: BDNF; C mechano-heat-sensitive: CMH; atonal homolog 1a: *Atoh1*; cartwheel

cells: CWCs; the dorsal cochlear nucleus: DCN; double-strand break: DSB; single-guide RNAs: gRNA; Tetramethylrhodamine B isothiocyanate: TRITC; foramina nervosa: FN;

## Declarations

# Ethics approval and consent to participate

All animal procedures in this work were carried out in accordance with the Policy on Human Care and Use of Laboratory Animals at PLA General Hospital and approved by the Institutional Animal Care and Use Committee (process no. 2018-X14-84).

# Consent for publication

All authors have read the manuscript and indicated consent for publication.

# Availability of data and materials

All raw data generated during this study are included in this published article. The datasets during and/or analyzed during the current study available from the corresponding author on reasonable request.

# Competing interests

The authors declare that they have no competing interests.

# Funding

This work was supported by grants from the National Natural Science Foundation of China (NSFC #81670940), Key International (Regional) Joint Research Program of National Natural Science Foundation of China (NSFC#81820108009) and Special Cultivating and Developing Program of Beijing Science and Technology Innovation Base (z151100001615050).

# Authors' contributions

Mian Zu, Wei-guo Shi, Shi-ming Yang designed the work. Wei-wei Guo interpreted data. Mian Zu, Tao Cong, Fei Ji, Shi-li Zhang performed experiments. Yue Zhang provided technical assistance. Xin Song, Mian Zu analyzed raw data. Shi-ming Yang, Wei Sun and David Z.Z. He substantively revised the manuscript. Mian Zu, Wei Sun wrote original draft. All authors read and approved the final manuscript.

# Acknowledgements

We thank Dr. Ning Yu (Chinese PLA Institute of Otolaryngology) and Qing Chang (CasGene Biotech.Co., Ltd) for technical supports.

# References

1. Akopian AN, Sivilotti L, Wood JN. A tetrodotoxin-resistant voltage-gated sodium channel expressed by sensory neurons. Nature. 1996;379(6562):257–62.
2. Dib-Hajj SD, Tyrrell L, Waxman SG. Structure of the sodium channel gene SCN11A: evidence for intron-to-exon conversion model and implications for gene evolution. Mol Neurobiol. 2002;26(2–3):235–50.
3. Tyrrell L, Renganathan M, Dib-Hajj SD, Waxman SG. Glycosylation alters steady-state inactivation of sodium channel Nav1.9/NaN in dorsal root ganglion neurons and is developmentally regulated. J Neurosci. 2001;21(24):9629–37.
4. Xu W, Zhang J, Wang Y, Wang L, Wang X: **Changes in the expression of voltage-gated sodium channels Nav1.3, Nav1.7, Nav1.8, and Nav1.9 in rat trigeminal ganglia following chronic constriction injury**. *Neuroreport* 2016, **27**(12):929–934.
5. Thun J, Persson AK, Fried K. Differential expression of neuronal voltage-gated sodium channel mRNAs during the development of the rat trigeminal ganglion. Brain Res. 2009;1269:11–22.
6. O'Donnell AM, Coyle D, Puri P. Decreased Na(v)1.9 channel expression in Hirschsprung's disease. J Pediatr Surg. 2016;51(9):1458–61.
7. O'Brien BJ, Caldwell JH, Ehring GR, O'Brien KMB, Luo SJ, Levinson SR. Tetrodotoxin-resistant voltage-gated sodium channels Na(v)1.8 and Na(v)1.9 are expressed in the retina. J Comp Neurol. 2008;508(6):940–51.
8. Delmas P, Coste B. Na + channel Nav1.9: in search of a gating mechanism. Trends in neurosciences. 2003;26(2):55–7.
9. Blum R, Kafitz KW, Konnerth A. Neurotrophin-evoked depolarization requires the sodium channel Na(V)1.9. Nature. 2002;419(6908):687–93.
10. Baker MD, Chandra SY, Ding Y, Waxman SG, Wood JN. GTP-induced tetrodotoxin-resistant Na + current regulates excitability in mouse and rat small diameter sensory neurones. J Physiol. 2003;548(Pt 2):373–82.
11. Cummins TR, Dib-Hajj SD, Black JA, Akopian AN, Wood JN, Waxman SG. A novel persistent tetrodotoxin-resistant sodium current in SNS-null and wild-type small primary sensory neurons. J Neurosci. 1999;19(24):1713–4.
12. Huang J, Vanoye CG, Cutts A, Goldberg YP, Dib-Hajj SD, Cohen CJ, Waxman SG, George AL Jr. Sodium channel NaV1.9 mutations associated with insensitivity to pain dampen neuronal excitability. J Clin Investig. 2017;127(7):2805–14.

13. Hoffmann T, Kistner K, Carr RW, Nassar MA, Reeh PW, Weidner C: **Reduced excitability and impaired nociception in peripheral unmyelinated fibers from Nav1.9-null mice**. *Pain* 2017, **158**(1):58–67.
14. Petitpre C, Wu HH, Sharma A, Tokarska A, Fontanet P, Wang YQ, Helmbacher F, Yackle K, Silberberg G, Hadjab S, et al: **Neuronal heterogeneity and stereotyped connectivity in the auditory afferent system**. *Nat Commun* 2018, 9.
15. Browne L, Smith K, Jagger D: **Identification of Persistent and Resurgent Sodium Currents in Spiral Ganglion Neurons Cultured from the Mouse Cochlea**. 2017, **4**(6):ENEURO.0303-0317.2017.
16. Lu J, Liu H, Lin S, Li C, Wu H. Electrophysiological characterization of acutely isolated spiral ganglion neurons in neonatal and mature sonic hedgehog knock-in mice. Neurosci Lett. 2019;714:134536.
17. Zhong C, Fu Y, Pan W, Yu J, Wang JF. Atoh1 and other related key regulators in the development of auditory sensory epithelium in the mammalian inner ear: function and interplay. Dev Biol. 2019;446(2):133–41.
18. Yoon H, Lee DJ, Kim MH, Bok J. Identification of genes concordantly expressed with Atoh1 during inner ear development. Anatomy cell biology. 2011;44(1):69–78.
19. Yan Z, Xu Y, Liang M, Ren X. Expression and functional role of Nav1.9 sodium channel in cartwheel cells of the dorsal cochlear nucleus. Mol Med Rep. 2015;11(3):1833–6.
20. Zu M, Yang F, Zhou WL, Liu AL, Du GH, Zheng LS. In vitro anti-influenza virus and anti-inflammatory activities of theaflavin derivatives. Antivir Res. 2012;94(3):217–24.
21. Stankovic KM, Corfas G. Real-time quantitative RT-PCR for low-abundance transcripts in the inner ear: analysis of neurotrophic factor expression. Hearing Res. 2003;185(1–2):97–108.
22. Wan GQ, Corfas G. **Transient auditory nerve demyelination as a new mechanism for hidden hearing loss**. *Nat Commun* 2017, 8.
23. Chen W, Hao QQ, Ren LL, Ren W, Lin HS, Guo WW, Yang SM. **Cochlear morphology in the developing inner ear of the porcine model of spontaneous deafness**. *Bmc Neurosci* 2018, 19.
24. Landry TG, Wise AK, Fallon JB, Shepherd RK. Spiral ganglion neuron survival and function in the deafened cochlea following chronic neurotrophic treatment. Hear Res. 2011;282(1–2):303–13.
25. Wrzeszcz A, Reuter G, Nolte I, Lenarz T, Scheper V. Spiral ganglion neuron quantification in the guinea pig cochlea using Confocal Laser Scanning Microscopy compared to embedding methods. Hearing Res. 2013;306:145–55.
26. Zu M, Jiang J, Zhao H, Zhang S, Yan Y, Qiu S, Yuan S, Han J, Zhang Y, Guo W, et al. Rapid analysis of neomycin in cochlear perilymph of guinea pigs using disposable SPE cartridges and high performance liquid chromatography-tandem mass spectrometry. Journal of chromatography B Analytical technologies in the biomedical life sciences. 2018;1093–1094:52–9.
27. Chen L, Guo W, Ren L, Yang M, Zhao Y, Guo Z, Yi H, Li M, Hu Y, Long X, et al. A de novo silencer causes elimination of MITF-M expression and profound hearing loss in pigs. BMC Biol. 2016;14:52.
28. Dib-Hajj SD, Black JA, Waxman SG. NaV1.9: a sodium channel linked to human pain. Nat Rev Neurosci. 2015;16(9):511.

29. Nitecka LM, Sobkowicz HM. The GABA/GAD innervation within the inner spiral bundle in the mouse cochlea. Hearing Res. 1996;99(1–2):91–105.
30. Kim KX, Rutherford MA. Maturation of NaV and KV Channel Topographies in the Auditory Nerve Spike Initiator before and after Developmental Onset of Hearing Function. Journal of Neuroscience the Official Journal of the Society for Neuroscience. 2016;36(7):2111.
31. Maxeiner S, Luo FJ, Tan A, Schmitz F, Sudhof TC. How to make a synaptic ribbon: RIBEYE deletion abolishes ribbons in retinal synapses and disrupts neurotransmitter release. Embo J. 2016;35(10):1098–114.
32. Wan GQ, Gomez-Casati ME, Gigliello AR, Liberman MC, Corfas G. **Neurotrophin-3 regulates ribbon synapse density in the cochlea and induces synapse regeneration after acoustic trauma**. *Elife* 2014, 3.
33. Wilson-Gerwing TD, Stucky CL, Mccomb GW, Verge VMK. Neurotrophin-3 significantly reduces sodium channel expression linked to neuropathic pain states. Exp Neurol. 2008;213(2):303–14.
34. Hossain WA, Antic SD, Yang Y, Rasband MN, D Kent M. Where is the spike generator of the cochlear nerve? Voltage-gated sodium channels in the mouse cochlea. Journal of Neuroscience the Official Journal of the Society for Neuroscience. 2005;25(29):6857.
35. Celaya AM, Sanchez-Perez I, Bermudez-Munoz JM, Rodriguez-de la Rosa L, Pintado-Berninches L, Perona R, Murillo-Cuesta S, Varela-Nieto I: **Deficit of mitogen-activated protein kinase phosphatase 1 (DUSP1) accelerates progressive hearing loss**. *Elife* 2019, **8**.
36. François M, Bertrand C, Françoise P, Nadine C, Marcel C, Korogod SM, Patrick D. Inflammatory mediators increase Nav1.9 current and excitability in nociceptors through a coincident detection mechanism. The Journal of General Physiology. 2008;131(3):211–25.

# Figures

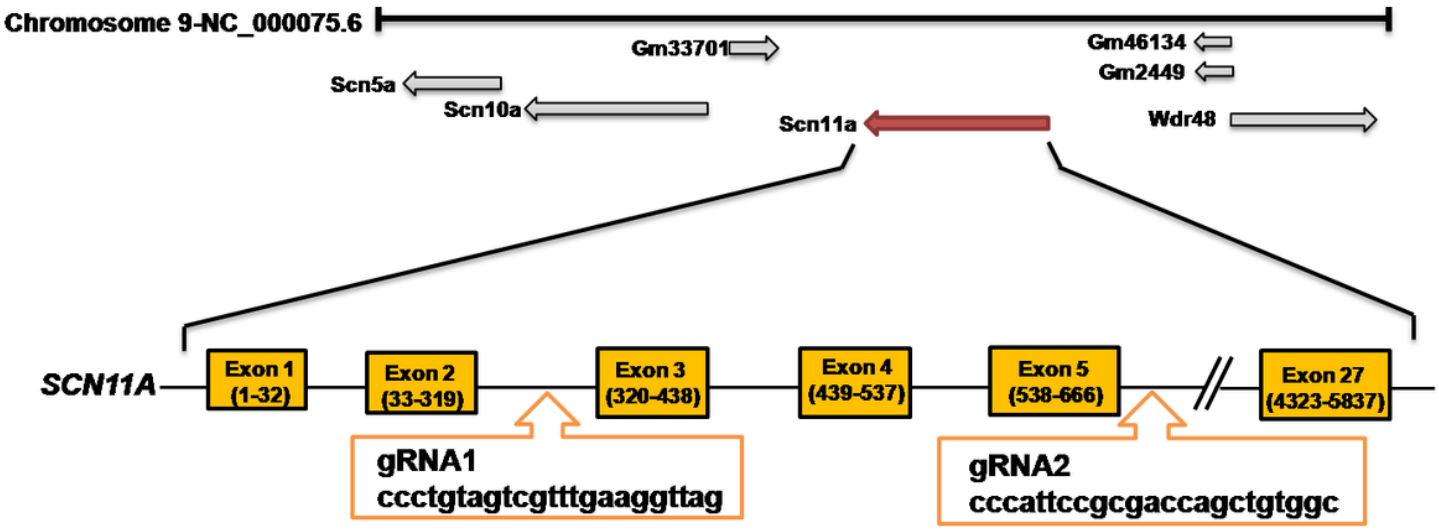


Figure 1

A representative illustration of the CRISPR/Cas9 targeting strategy for generating Nav1.9 knockout (KO) mice. The Cas9 mRNA and two single guide RNAs targeting a region from SCN11A exon 3 to 5, were microinjected into mouse zygotes.

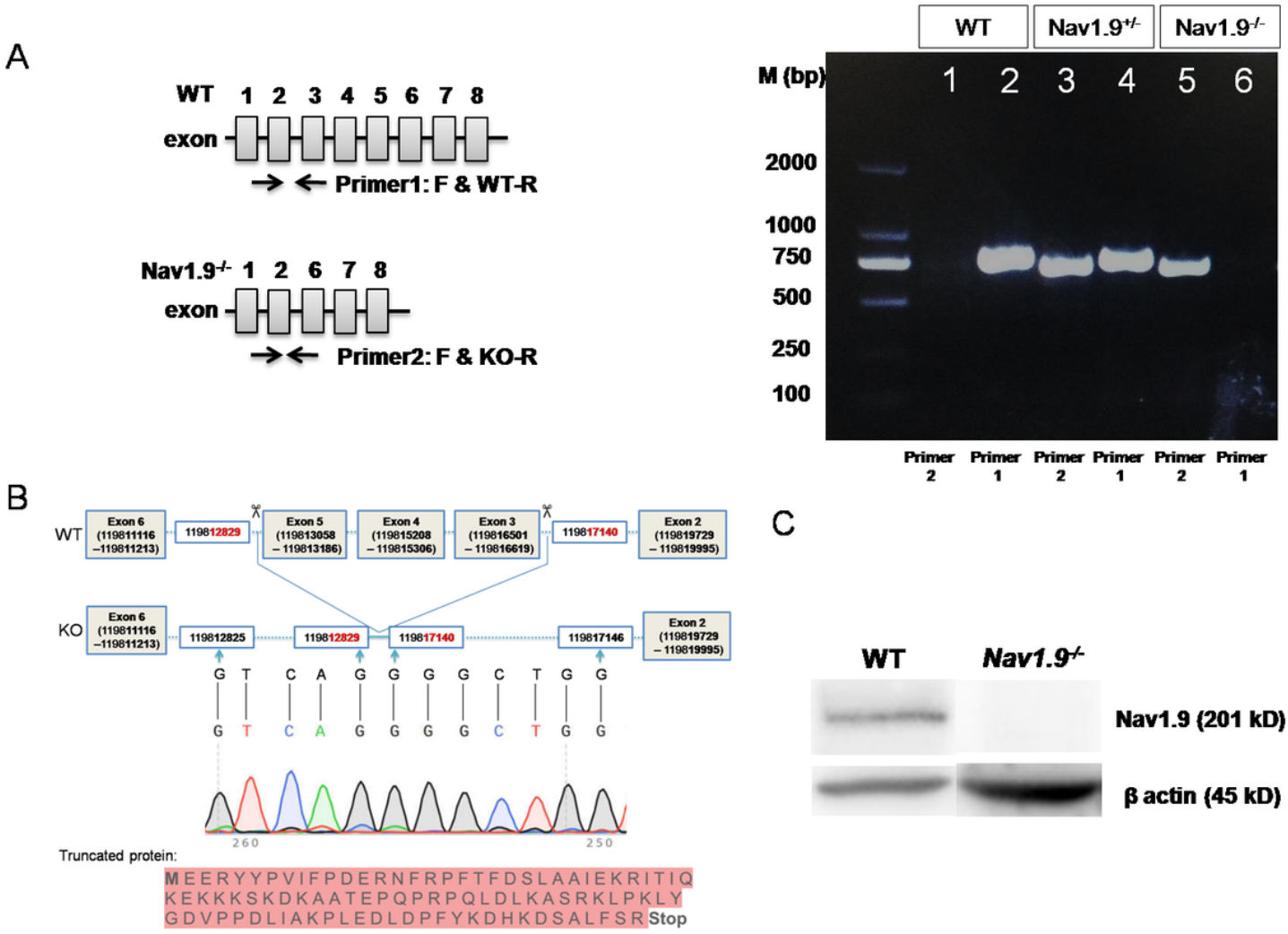


## Figure 2

CRISPR/Cas 9-mediated generation of a Nav1.9-/- mouse model. A, Schematic diagram of primer pair design for PCR genotyping, a representative PCR genotyping result for Nav1.9 wild-type (WT), homozygous (Nav1.9 -/-) and heterozygous (Nav1.9 +/-), the region of junction of DSB is absent in the WT mice. B, This successfully eliminated all of exon 3, 4 and 5, as confirmed by Sanger sequencing, induces reading frame shift and thus a premature translational- termination codon during the truncated protein expression. C, Nav1.9 protein expression in the cochlea of Nav1.9-/- mice were compared to WT.

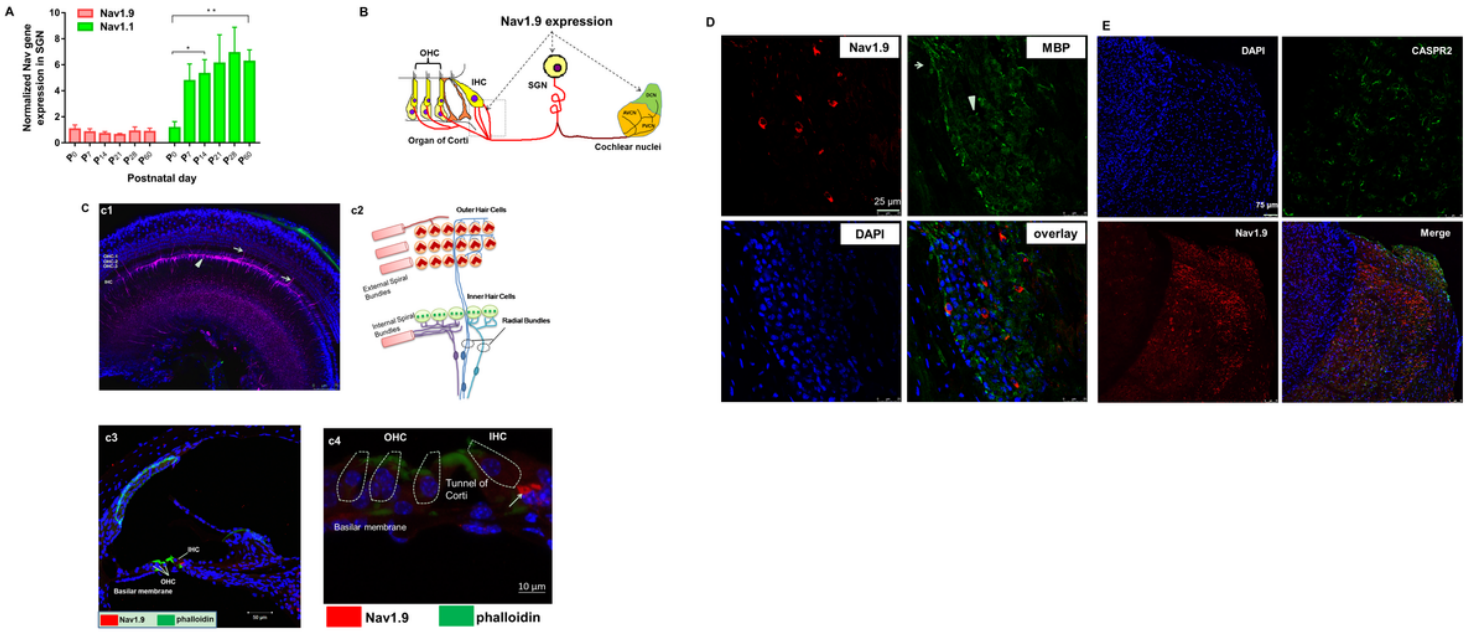


## Figure 3

Distribution of Nav1.9 in primary auditory afferents. A, The voltage-gated sodium channel Nav1.9 and Nav1.1 mRNA levels in modiolus of WT ICR mice at the postnatal 0, 7th, 14th, 21th, 28th and 60th day. Each time point contains 5 mice. *p=0.028, **p=0.004. B, A schematic representing the localization of Nav1.9 channels at primary afferent peripheral nerve endings on hair cells in cochlea, in SGN somata, in the auditory nerve located within the modiolus, and in the cochlear nuclei. C, Nav1.9 is present in cochlea basilar membrane by surface preparation technique and immunofluorescence staining in cryo-section. c1, Horizontal section showing three rows of OHCs and one row of IHCs. In a linear distribution below the IHCs, Nav1.9 (purple) is in the afferent endings beneath the IHC bases. Also stained are the afferent radial fibers leading through the tunnel of Corti to their first hemi-nodes beneath the foramina nervosa. Scales=75 μm. c2, the diagram of the cochlea's afferent innervations pattern. c3, Nav1.9 is in the nerve endings of internal spiral fibers or radial fibers beneath IHC (red), the cilia of which exhibit phalloidin labeling (green). Scales=50 μm. c4, the high magnification image of c3. Scale= 10 μm. D, Expression of Nav1.9 in the SGNs of P60 WT mouse. Nav1.9, MBP, and cell nucleus are stained as red, green and blue. E, Some neurons from the dorsal cochlear nucleus are labeled by Nav1.9 (red).

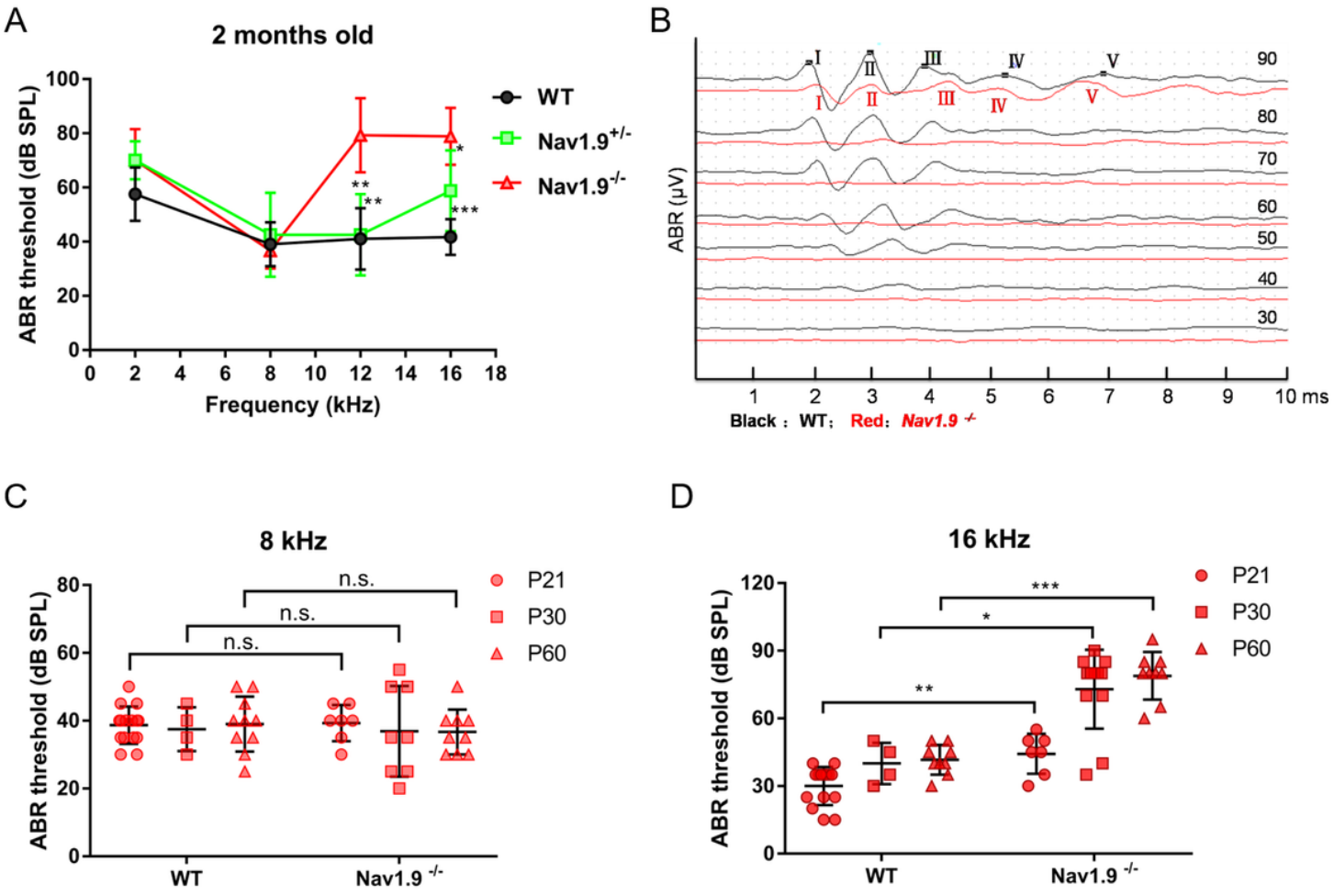


## Figure 4

Audiological characterization of Nav1.9-/- mice. A, Mean ABR thresholds of six wild-type, four heterozygous and seven homozygous versus sound frequency, **p=0.002, **p=0.001 at 12 kHz compared with homozygous, *p=0.01, ***p=0.000 at 16 kHz compared with homozygous by one-way ANOVA with Bonferroni's post-hoc test. B, Example of ABR waveforms at 16 kHz in one ear of a wild-type superimposed on an example of ABR waveforms in one ear of Nav1.9-/- mice. C, Mean ABR threshold of WT and homozygous mice of postnatal day 21 to 60 at 8 kHz. p=0.807 at P21; p=0.932 at P30; p=0.504 with independent samples t test; n.s.: not significant. D, Mean ABR threshold of wild-type and homozygous mice of postnatal day 21 to 60 at 16 kHz. *p=0.016, **p=0.006, ***p=0.000 with Mann-Whitney test. Data are expressed as mean±s.d.

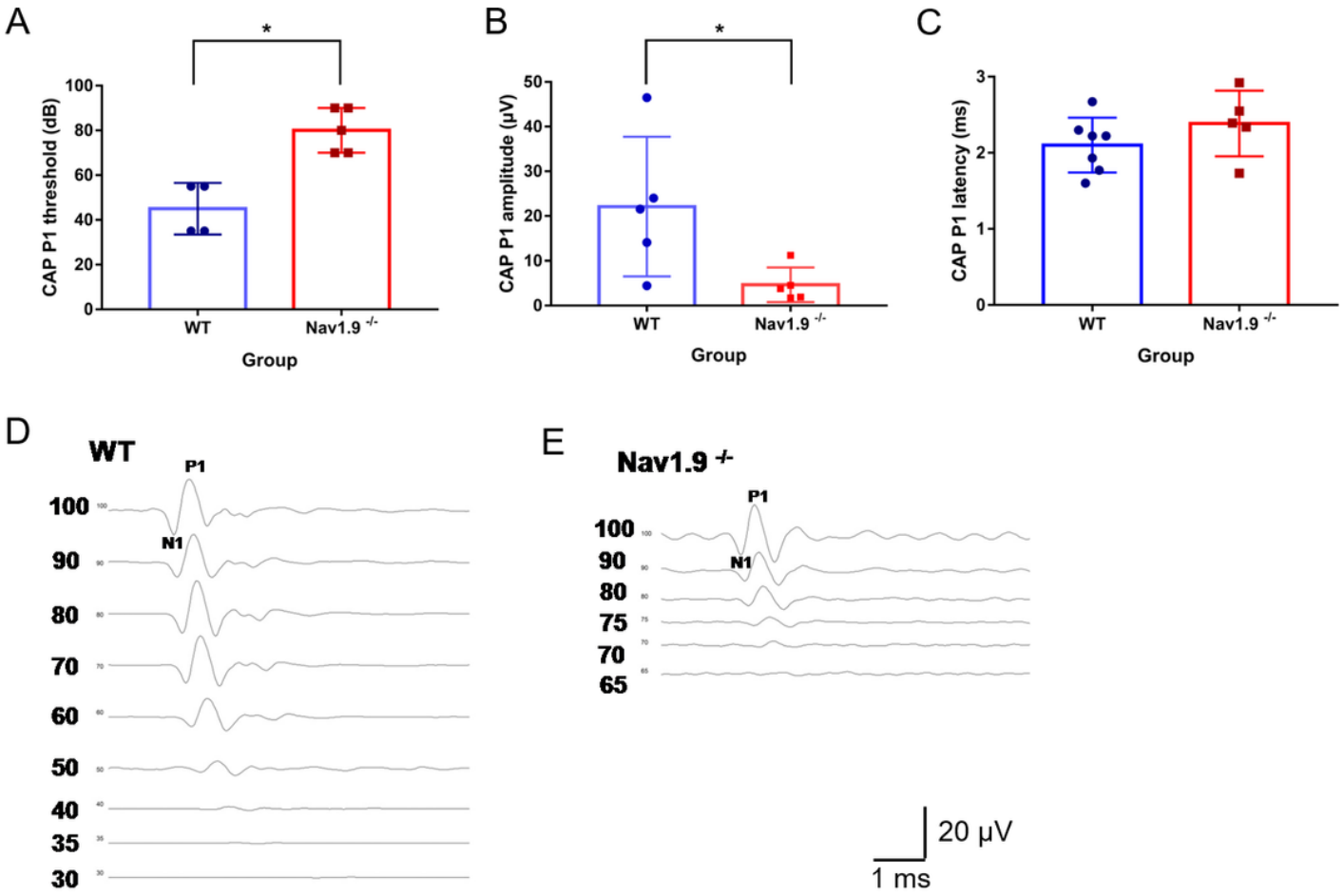


## Figure 5

Auditory compound action potentials are affected by Nav1.9 knockout. Nav1.9 knockout induces higher CAP P1 thresholds, *p=0.013 with Mann-Whitney test (A), lower CAP P1 amplitudes, *p=0.041 with independent samples t test (B), compared with their WT littermates; C, the averaged CAP P1 latencies are not affected at the time point of postnatal day 60, p=0.242 with independent samples t test. D, example of CAP waveforms in one ear of WT mice. E, example of CAP waveforms in one ear of Nav1.9-/- mice. Data are expressed as mean±s.d.

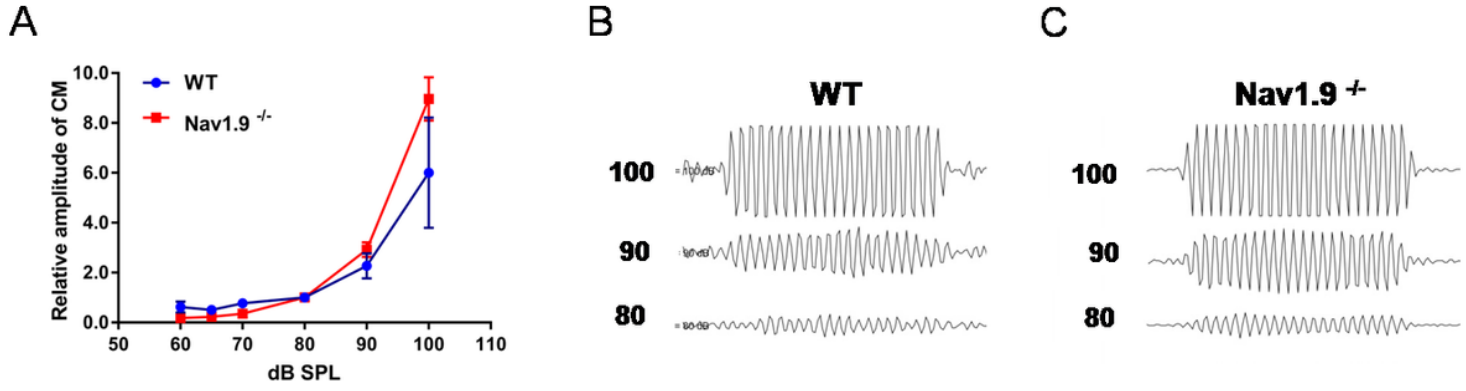


## Figure 6

Cochlear microphonic (CM) potentials are unaffected by Nav1.9 knockout. A, the input-output function in response to 4 kHz. B, example of CM waveforms in one ear of wild-type mice. B, example of CM waveforms in one ear of Nav1.9-/- mice.

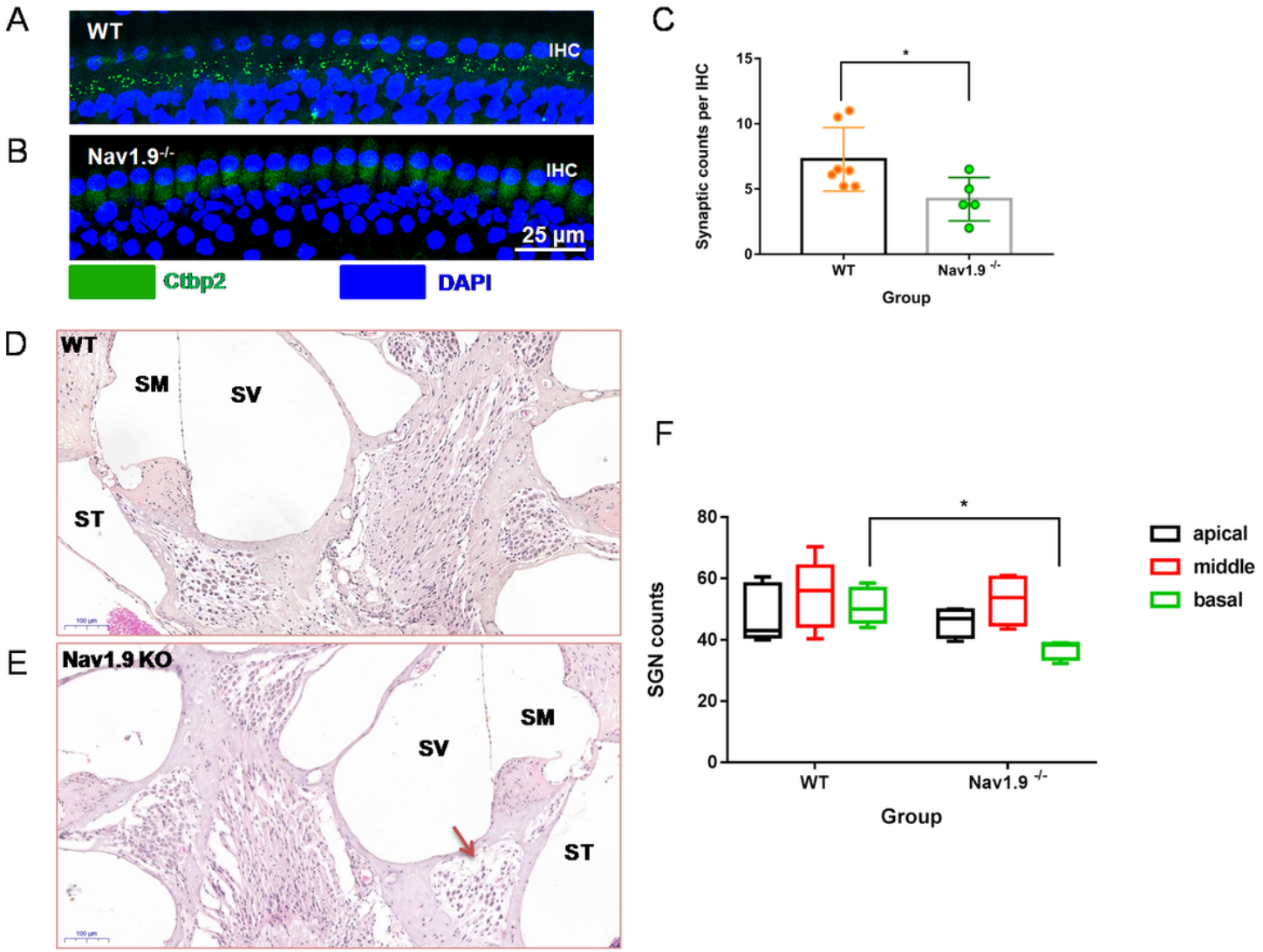


## Figure 7

Nav1.9 knockout affects ribbon synapse density and survival of spiral ganglion neurons. Representative images of ribbon synapses immunostained with Ctbp2 (green) from WT (A) and Nav1.9-/- mice (B). C, Quantitative analysis of ribbon synapse counts per IHC from five randomly selected visual fields for each mouse. n=7 for WT group, n=5 for Nav1.9-/- group. *p=0.034 by Mann-Whitney test. Representative images of spiral ganglion neurons in Rosenthal's canal from WT (D) and Nav1.9-/- mice (E). F, Spiral ganglion neuron counts in the basal turn, the middle turn and apical turn together in 3 midmodiolar sections for each animal. n=5 for WT group, n=4 for Nav1.9-/- group. *p=0.014 by Mann-Whitney test. Data are expressed as mean±s.d.

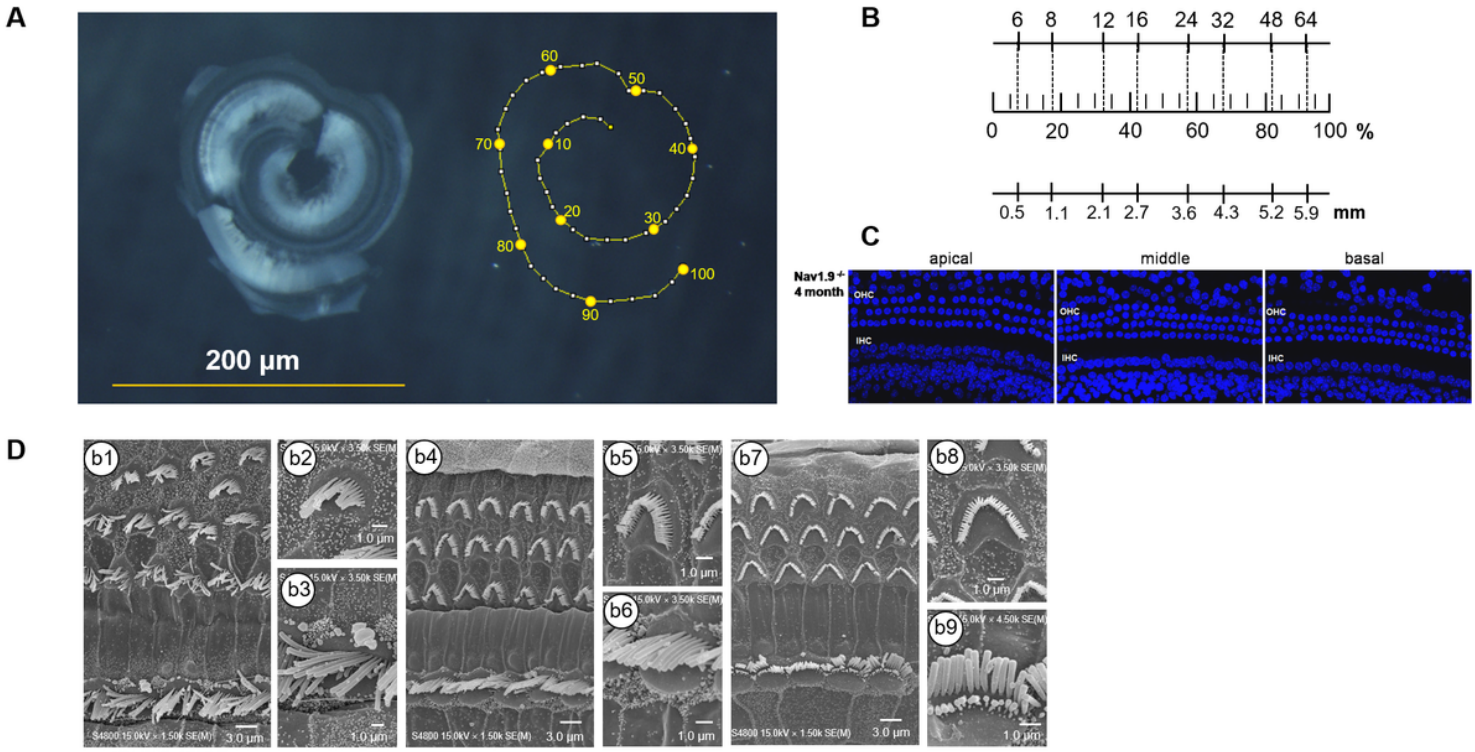


**Figure 8**

Nav1.9 knockout does not affect the morphology of hair cells. A, The digital image of a dissected 4 months old mouse cochlea including the hook region (left). Schematic drawing of the same cochlea with percent distance from the apex plotted (right). B, Scale is showing frequency, percent distance from the apex, and distance (mm), according to Müller (2004): x=100-(156.53-82.46*log(F)). The full basilar membrane length is 6.3 mm for this particular cochlea. C, Images of organ of Cortis from 4 months old mice stained by DAPI (blue), with the apical turn (0-25% distance from the apex), the middle turn (30-55% distance from the apex) and the basal turn (60-85% distance from the apex) D, Images of the organ of Corti of Nav1.9-/- mice at postnatal ages of 2 months by SEM, containing the apical turn (b1-b3), the middle turn (b4-b6), and the basal turn (b7-b9).

# Supplementary Files

This is a list of supplementary files associated with this preprint. Click to download.

- AuthorChecklistFull.pdf
- Additionalfile.docx
- figS1.png
- figS2.png
- figS3.png